JOURNAL OF MATERIALS SCIENCE 12 (1977) 1573–1586

Impact of small steel spheres on glass surfaces

C. G. KNIGHT, M. V. SWAIN, M. M. CHAUDHRI
Physics and Chemistry of Solids Group, Cavendish Laboratory, Cambridge, UK

A high speed photographic study has been made as part of a detailed investigation of the impact of small steel spheres (~ 800 and 1000 μm diameter) on to Pyrex and soda-lime glasses. The velocity of the spheres was varied from 20 to 300 m sec^{-1} and the fracturing process during the complete impact cycle was followed. Observations revealed substantial differences in the behaviour of the two glasses, particularly at higher velocities; Pyrex behaved as though indented by a sphere, whereas soda lime glass behaved as though indented with a pointed indenter. As with quasi-static pointed indentations, cracking was observed during the unloading cycle. It was also found that the angle of the Hertzian cone crack in Pyrex glass varied in a systematic manner with velocity. Rebound velocity, time of contact and extent of flattening of the steel spheres were also recorded. The relevance of these observations to impact erosion and strength degradation of brittle materials is pointed out.

1. Introduction

The response of brittle solids to impact by solid and quasi-solid particles is a subject of considerable interest because of its significance to problems of erosion and strength degradation of this important class of materials. Previous work by Andrews [1], Longchambon [2] and Tillet [3] established that for a sphere of given diameter there existed a critical velocity or drop height to nucleate a cone crack in a given glass. Roesler [4] was able to show that this observation was simply a restatement of the fact that under quasi-static conditions the critical load to initiate a cone crack was proportional to the indenter radius, so-called Auerbach's law [5]. However, for velocities greatly in excess of the velocity to initiate cone cracks, crushing and the formation of a variety of other cracking systems occur. These types of cracks have been described by Tsai and Kolsky [6], and Cherepanov and Sokolinsky [7], primarily from post impact microscopic examination. Previous work on indentation fracture by Lawn and Swain [8], and Swain and Hagan [9] has highlighted the importance of observing the fracturing process during loading and unloading of the indenter. Only in this manner can the separate stages of the fracture process be identified and correctly related to the state of loading and stress field at a particular time.

Other studies of the impact of brittle solids with high velocity solid and liquid particles have shown that dynamic effects can also play an important role. Bowden and Field [10], and Field [11] have shown that when a lead slug or high velocity water jet strikes a brittle solid, microcracks well away from the impact site may be opened up by the surface Rayleigh wave produced. Recently Glenn [12], studying the impact of glasses with steel cylinders, has proposed that the interaction of the impact stresses with the reflected compressive stress pulse plays a significant role in the microfracture beneath the impact site.

This paper describes and discusses the results of dynamic indentations of float (soda-lime silicate) and Pyrex (borosilicate) glasses by 0.8 and 1.0 mm hardened steel balls at up to 300 m sec^{-1}. In the course of this investigation we have studied the actual sequence of damage formation using high-speed photography, and see that it is a two-stage process similar to the quasi-static pointed inden-

tation case. However, a considerable difference in the behaviour of these two traditionally model brittle materials was observed. The response of the soda-lime glass (particularly above $\sim 160\,\mathrm{m\,sec^{-1}}$ with a 1 mm ball) was as if indented with a sharp indenter, whereas the Pyrex glass behaved as if indented with a spherical indenter under quasi-static conditions. These differences are thought [9] to arise because of the small amount of plastic deformation which occurs in soda-lime glass when indented with small spheres.

Other important observations to emerge from this study were: systematic variation of cone crack angle with incident particle velocity in Pyrex glass; determination of the coefficient of restitution and the time of contact of the impacting sphere; determination of the depth of damage during impact and its comparison with recent quasi-static theories; and finally the flat diameter on the sphere as a function of impacting velocity.

2. Theoretical considerations

2.1. Elastic loading

The elastic contact between curved bodies was first analysed by Hertz [13] in 1881. The original analysis gave explicit considerations to contact diameter and surface stresses. Subsequent work by Huber [14] determined the stresses within the indented elastic half space.

For a sphere of radius R in contact with a flat under a normal load P, the radius of contact is given by

$$a^3 = \tfrac{3}{4}kPR \qquad (1)$$

where $k = \left(\frac{1-\nu_1^2}{E_1} + \frac{1-\nu_2^2}{E_2}\right)$, E_1, ν_1 and E_2, ν_2 are Young's moduli and Poisson's ratio respectively. The distance of mutual approach z between contacting bodies is given by

$$z = a^2/R \qquad (2)$$

Provided that the contact circle expands at a rate less than the velocity of elastic waves, a quasi-static analysis provides a very good description of the stresses during dynamic contact [22]. The above expressions may be formulated in terms of the velocity of the impacting particle by equating P and V. To derive a relationship between P and V, the kinetic energy of the impacting sphere is equated to the strain energy at the time of maximum impression, that is

$$\tfrac{1}{2}(\tfrac{4}{3}\pi\rho R^3)V^2 = \int_0^{z_{\max}} P(z)\,\mathrm{d}z \qquad (3)$$

where ρ is the density of the sphere. Substituting for z from Equation 2 gives the equivalent maximum load

$$P_m = (\tfrac{5}{3}\pi\rho)^{3/5}(\tfrac{3}{4}k)^{-2/5}V^{6/5}R^2. \qquad (4)$$

Within the diameter of contact the applied load is distributed as a hemisphere of compressive stress which depresses the surface of the solid and flattens the indenter. In addition there are tangential elastic surface displacements within the area of contact which are directed radially towards the axis of contact. These displacements are responsible for the tensile surface radial stress σ_r and compressive hoop stress σ_θ, these stresses are given by

$$\sigma_r = \frac{(1-2\nu_1)}{2\pi}\frac{P}{r^2} = \frac{(1-2\nu_1)}{2}p_0\left(\frac{a}{r}\right)^2 = -\sigma_\theta; \qquad r \geqslant a \qquad (5)$$

where r is the radial distance from the axis of contact, and p_0 is the mean indentation pressure. The maximum tensile stress occurs at the edge of the contact circle provided there is no mismatch of elastic constants giving rise to differential elastic surface displacements. This effect has been recently treated by Johnson *et al.* [15] and their analysis indicates that σ_r may reach a maximum way from the contact edge. The maximum shear stress occurs beneath the area of contact at a depth 0.5 a along the contact axis and has a maximum value of 0.45 p_0 (depending upon ν) where p_0 is the mean indentation pressure. A more complete description of the stresses beneath a spherical indenter has been given in a recent review by Lawn and Wilshaw [16].

2.2. Inelastic loading

On increasing the load or impact velocity the subsurface shear stress exceeds the yield stress and plastic deformation of the sphere or flat will occur. In the case of a brittle material, crushing may occur above a critical threshold stress. In both cases the Hertzian elastic analysis breaks down and an exact analytical expression of the stresses becomes complex. Some progress may be made upon the introduction of certain simplistic assumptions in the case of an ideal elastic–plastic material.

Following a proposal by Marsh [17] the formation of a permanent impression may be likened to

the expansion of a spherical cavity by a uniform hydrostatic pressure in an infinite solid. The stresses about the cavity have been determined by Hill [18] and outside the plastic zone are given by

$$\left.\begin{aligned}\sigma_r &= -\frac{2Y}{3}\left(\frac{c}{r}\right)^3 \\ \sigma_\theta &= \frac{Y}{3}\left(\frac{c}{r}\right)^3\end{aligned}\right\} \quad r>c \qquad (6)$$

where Y is the yield stress and c the plastic boundary. Equation 6 is strictly only true for a spherical cavity under internal pressure. A better approximation on the surface outside the area of contact has been proposed by Puttick *et al.* [19] as the expansion of a hole in a plate by internal pressure. The stresses outside the plastic zone in this case are given by

$$\sigma_\theta = -\sigma_r = \frac{Y}{\sqrt{3}}\left(\frac{c}{r}\right)^2; \qquad r>c \qquad (7)$$

The significant difference between the elastic and inelastic loading stresses is that they are opposite in sign. A more complete description of the plastic loading stresses and their role in fracture initiation during unloading has been given elsewhere [9, 33].

When crushing occurs and a zone of crushed material resides between the indenter and uncrushed glass the problem is similar to that of crushed rocks about tunnels which has been treated by Jaeger [20]. Jaeger's analysis is very similar to that in an elastic–plastic solid, only the yield stress Y in the previous two equations is replaced by S the shear strength of the crushed glass.

2.3. Duration of contact and coefficient of restitution

For the purely elastic case, the contact time t for a sphere of radius R striking a flat is given by [21]

$$t = 2.94\left(\frac{5\rho\pi k}{4}\right)^{2/5}\frac{R}{V^{1/5}} \qquad (8)$$

where V is the impact velocity and ρ the density of the sphere. This relationship will hold until plastic deformation or crushing of the ball or substrate occur. The critical impact velocity to initiate plastic deformation may be determined by relating the mean indentation pressure p_0 to the yield stress Y. That is

$$p_0 = \frac{P_M}{\pi a^2} \simeq Y \qquad (9)$$

where a is the radius of contact and P_M is the equivalent maximum load given by Equation 6. The above equation explicitly assumes that the yield stress is independent of strain rate or velocity of impact. Upon exceeding the yield stress, Andrews [1] has proposed that the contact time is independent of velocity, and the diameter of the flat produced by permanent deformation at speeds above the critical velocity are proportional to the square root of the velocity. When crushing occurs, the time of contact would be expected to increase because of the effectively low modulus of the crushed material beneath the sphere.

The rebound velocity of a sphere with a flat is always less than the impact velocity. This energy loss on impact has been attributed by Hunter [22] to elastic wave dispersion, internal friction and hysteresis of the materials. In the present case futher energy loss occurs upon fracture of the glass and/or plastic deformation of the sphere. When crushing occurs the low effective modulus of the glass will further reduce the coefficient of restitution.

3. Indentation fracture

In this section, a short review of the various types of fracture that occur during quasi-static indentations with spherical indenters is presented.

3.1. Cone cracking

When a spherical indenter in contact with a brittle material is loaded above a critical load, a so-called cone crack initiates just outside the area of contact and propagates into the material. Auerbach [5] observed that for a particular glass the critical load P_c was related to the indenter radius R, that is

$$P_c = AR \qquad (10)$$

where A is a constant, often called Auerbach's constant. Equation 10 has been subsequently verified by many authors for a wide range of crystalline and non-crystalline brittle materials with a variety of surface preparations. Equation 10 may be rewritten in terms of impact velocity or drop height of a sphere. An expression for the critical velocity to initiate a cone crack, provided there are no environmental effects, is from Equations 4 and 10

$$V_c = A''/R^{5/6} \qquad (11)$$

where

$$A'' = \left[\frac{A}{(\frac{5}{3}\pi\rho)^{5/3}(\frac{3}{4}k)^{-2/5}}\right]^{5/6}.$$

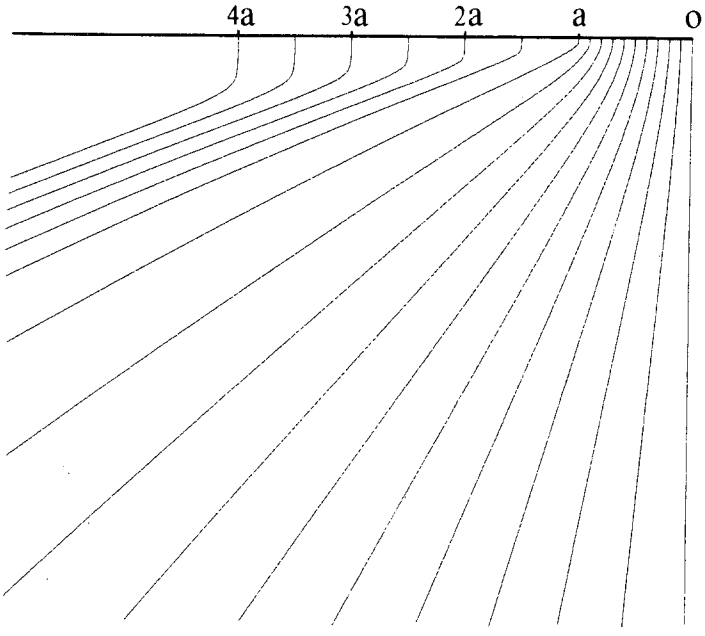

Figure 1 Side view of stress trajectories in Hertzian stress field. Plotted for $\nu = 0.33$. **oa** denotes radius of contact.

Equation 10, which violates the critical stress criterion (that is, when $\sigma_r = \sigma_{crit}$ or from Equation 3 $P_c \propto R^2$), has provoked many explanations. The two most popular are a flaw statistics approach [23] and a fracture mechanics approach [24]. The former is probably valid when the number and dimensions of the surface flaws are very small, whereas the latter provides a more satisfactory analysis when the reverse is true. However, as most surfaces have a proliferation of surface flaws unless carefully handled or treated the latter approach provides a simple and conservative basis upon which to design brittle materials subject to impact.

Once a cone crack has initiated, subsequent growth follows the tensile stress trajectories into the solid. A plot of the tensile stress trajectories is shown in Fig. 1. These trajectories are such that tangents and normals to the the curves at any point indicate the directions of the principal stresses. Normally once the area of contact has encompassed the surface trace of the cone crack it ceases to grow. However in the case of impact, as will be seen in the following section, cone cracks within the area of contact continue to grow and as might be expected from Fig. 1 the resulting cone crack is steeper than for quasi-static indentations.

The stress trajectories in Fig. 1 were obtained from the stress analysis by Huber [14] using a Poisson's ratio of 0.33, rather than 0.22, for the glass. Only with this value of Poisson's ratio did the cone crack trajectories agree with quasi-static observations of the cone crack angle. A similar procedure was adopted by Lawn *et al.* [25] in a computer simulation study of Hertzian fracture. These authors rationalized this approach because of variations of Poisson's ratio with hydrostatic pressure of glasses as observed by Mallinder and Proctor [26].

On unloading cone cracks usually close up unless crushing has occurred and then a slight turn up of the rim of the cone crack occurs [3]. Occassionally cone cracks are observed to form on unloading, Johnson *et al.* [15] have recently proposed qualitative theoretical arguments to explain their occurrence.

3.2. Median, radial and lateral cracking

These types of cracks are normally observed during the loading and unloading cycle with pointed indenters. However, on loading with small spherical indenters, when plastic deformation hinders cone crack formation, "median" or normal (to the surface) cracks are observed to form under the indenter. The form of these cracks is similar to that occurring beneath pointed indenters on loading and is a penny shape below the compressive zone under the area of contact. Once formed these cracks continue to propagate in a stable manner on loading. Upon unloading "radial" cracks form within the surface about the area of contact at

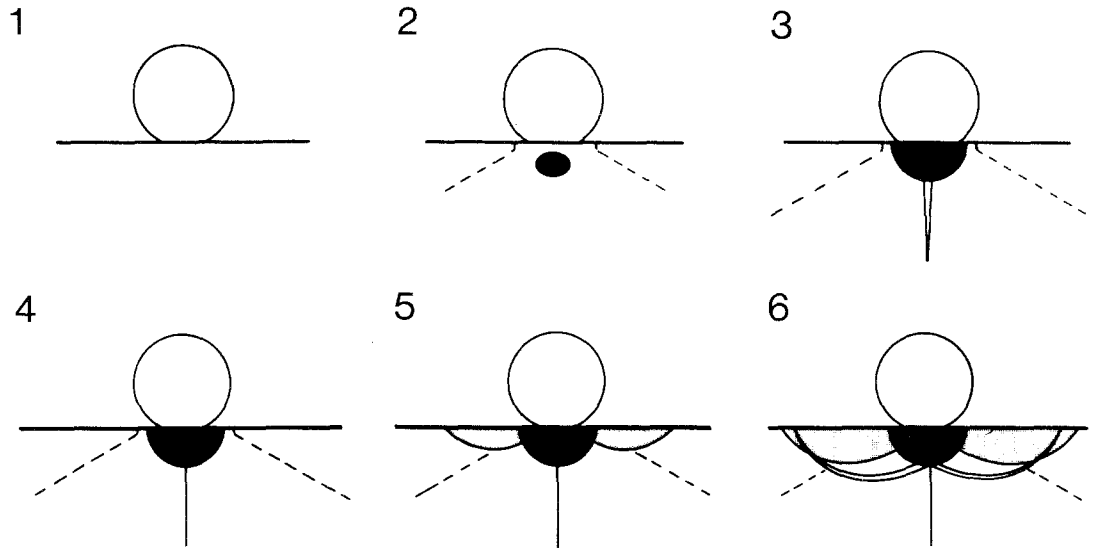

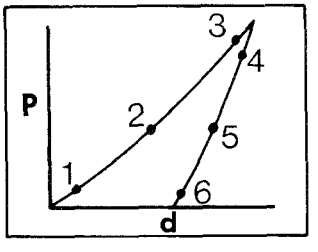

Figure 2 Schematic diagram of the cracking occurring during a quasi-static indentation with a small spherical indenter. Median cracks (MC) as well as plastic deformation (dark zone) and occasionally Hertzian cone cracks (CC) form during the loading cycle. Radial cracks (RC) and lateral cracks (LC) occur on the unloading cycle. The botton insert indicates the position on the load–displacment curve that each diagram refers to.

approximately half the maximum load. On continuing to unload another independent system of "lateral" cracks initiates just prior to complete unloading. This system of cracks initiates from the subsurface tension about the deformed zone and propagates in a saucer–like shape towards the surface. The general features of the fracturing about a small spherical indentation during loading and unloading are shown schematically in Fig. 2.

4. Experimental

4.1. Glasses and particles used

Commercially available soda-lime (float) glass and borosilicate (Pyrex) glass were selected for this study. Slabs typically 4 cm × 4 cm × 1 cm and 5 cm × 5 cm × 2.5 cm were polished until the surface was of optical quality. Impacts were usually made on the narrow edge of the blocks for photographic purposes and on the broad faces for other studies. Some tests were carried out on a fractured float glass surface but these were found to exhibit the same characteristics as the polished glasses although the scatter was greater.

The spheres were commercially available fully hardened steel ball bearings of 1.0 and 0.8 mm diameter. A few tests were carried out with smaller 0.4 mm diameter tungsten carbide spheres. The hardness of the steel spheres was $\simeq 9.2$ GPa. All spheres were cleaned of grease with acetone prior to impact on the glass.

4.2. Particle propulsion systems

Two different methods of propelling the spherical particles to high velocities were employed depending upon whether the damage was to be photographed with the high-speed camera or not. Because of the type of camera used, synchronisation of the particle firing mechanism and the camera had to be triggered electronically. To achieve this the particles were fired with the aid of a detonator beneath a thin brass plate upon which the spheres were placed. This method enabled excellent control of the firing time and reasonable control over the direction and velocity of the particles. The alternative method of propelling the particles was with a gas-gun [32]. This enabled the study to cover a wide velocity range, 20 to 300 m sec^{-1}, with excellent control over direction.

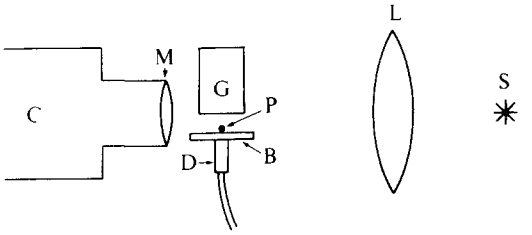

Figure 3 Schematic diagram of the high speed photography experimental arrangement. S, FA5 xenon filled flashtube; D, detonator; B, brass plate; P, projectile; G, glass block; M, microscope attached to the Beckman and Whitley model 189 rotating mirror framing camera, C; L, condenser lens.

4.3. High-speed photographic set-up

The camera used in this investigation was a Beckman and Whitley rotating mirror camera (model 189) capable of taking a sequence of 25 frames on standard 35 mm film at a rate of up to 4 million frames per second. The event was backlit with a Xenon filled flash tube of flash duration 150 μs. Synchronisation of the event, light flash, camera and particle firing mechanism was achieved electronically. A diagram of the camera set-up is shown in Fig. 3, but a more detailed account of the photographic details has been given elsewhere [27].

4.4. Time of contact and rebound velocity determination

Measurements of the contact time and rebound velocity were made during the impact study with the gas-gun. The duration of contact was determined by a high frequency (10 MHz) piezoelectric crystal (quartz) mounted behind the glass block.

The rebound velocity was determined with the aid of another peizoelectric crystal mounted on a steel plate at a known distance in front of the glass block. The particle was fired through a small hole in the steel plate on to the glass block which was inclined a few degrees ($< 5^{\circ}$) so that the rebounding particle would strike the steel plate. The impact on the glass triggered the oscilloscope and the arrival of the second pulse when the rebounding particle contacted the steel plate, could easily be detected and the time interval recorded. Velocities could be evaluated to accuracy of ~ 15%.

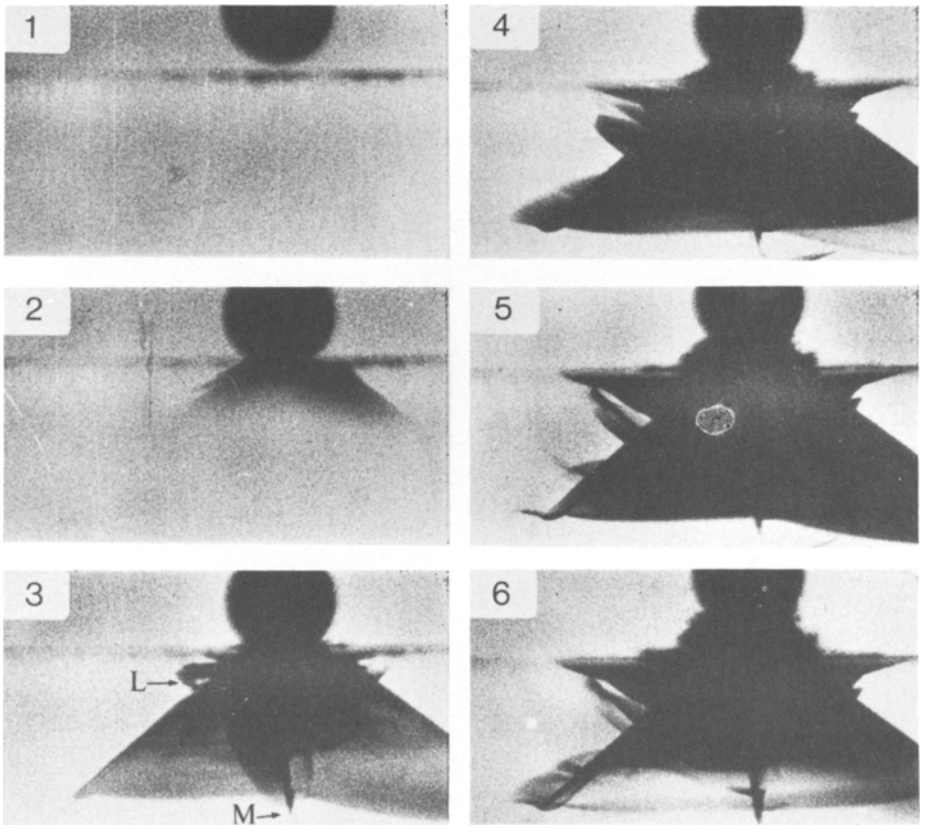

Figure 4 Impact of 1.0 mm diameter steel ball on Pyrex glass. Impact velocity ~ 200 m sec^{-1}; framing interval 1 μsec. Immediately after the impact a cone crack forms (frame 2) and then median M and lateral L cracks form (frame 3).

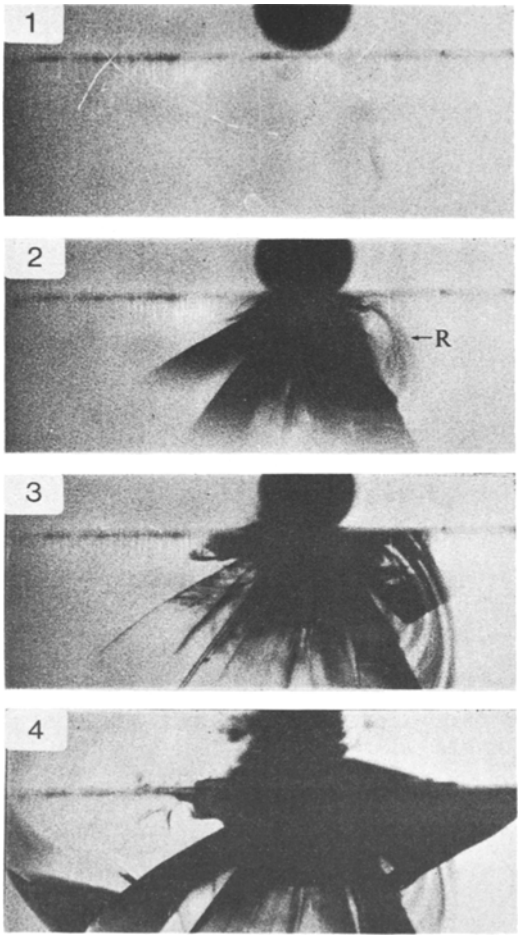

Figure 5 Impact of 1.0 mm diameter steel ball on Pyrex glass. Impact velocity $\sim 200\,m\,sec^{-1}$; framing interval 1 μsec.

5. Observations and discussion

5.1. High-speed photography

5.1.1. Pyrex glass

High-speed photographic sequences of impacts on polished surfaces of Pyrex glass are shown in Figs. 4 and 5. All sequences were taken at a rate of 1 million frames per second.

The most prominent feature of the damage to Pyrex glass is the formation of a well developed cone crack with an appearance similar to that developed during static loading. In Fig. 4 the cone crack appears to initiate well outside the contact diameter on one side, and then rapidly propagate about the contact site and into the glass. The cone crack has a semi-apex angle of $\sim 50°$ and propagates at ~ 1400 to $1500\,m\,sec^{-1}$. In frame 3 of Fig. 4 a distinct median crack M has formed. In contrast to soda-lime very little debris is ejected from the impact site during the initial stages of impact. Unloading results in the turning up of the cone crack towards the surface (frame 4) and the propagation of lateral cracks, L, from the sides of the cone crack towards the surface. Note also the sharp deviation ($\sim 90°$) of the median crack in frame 4 of Fig. 4 which continues to propagate for a short distance (~ 0.5 mm) parallel to the surface. A number of radial cracks also formed during the course of the impact.

In some cases it was observed that instead of a single cone crack multiple cone cracks formed. Fig. 5 shows such a sequence where an incomplete cone crack forms about the initial very steep inner cone crack (semi-apex angle $\sim 30°$). In this sequence the surface trace of the inner cone crack appears to be encompassed on continued loading and this presumably causes the initiation of the second cone crack. A radial crack *R* may also be seen to occur in frame 2 in Fig. 5. The cone crack speed in the early stages of the impact (frame 2) has reached a high value of 1800 to $1900\,m\,sec^{-1}$. It may also be seen in the same sequence that the cone cracks open (frame 2), close up (frame 3), and open again (frame 4). It is unlikely that this behaviour is due to the reflection of the stress waves, generated at the time of impact, from the other end of the block 40 mm from the impact site since the longitudinal wave velocity is about 5.5 $mm\,\mu sec^{-1}$. However, the possibility of interference of the release waves from the large faces (5 mm from the impact site) with the cracks formed, does exist.

5.1.2. Soda-lime glass

Examples of impact damage caused by impacts with 0.8 mm balls on to soda-lime glass are given in Fig. 6 and 7. Similar sequences were obtained with 1 mm balls only the damage was more extensive. The general features of all the impacts are very similar. After impact a large number of fine splinter cracks initiate beneath the impact site and propagate into the glass perpendicular to the maximum tensile stress trajectories. Sometimes a cone crack appears to initiate just prior to splinter crack development, see Fig. 6 frame 2. The formation of these splinter cracks is strikingly different from normal quasi-static indentations and impact damage with Pyrex. For elastic contact the zone directly beneath the area of contact is highly compressive and normally is unlikely to induce tensile fracture. There is a weak zone of tension

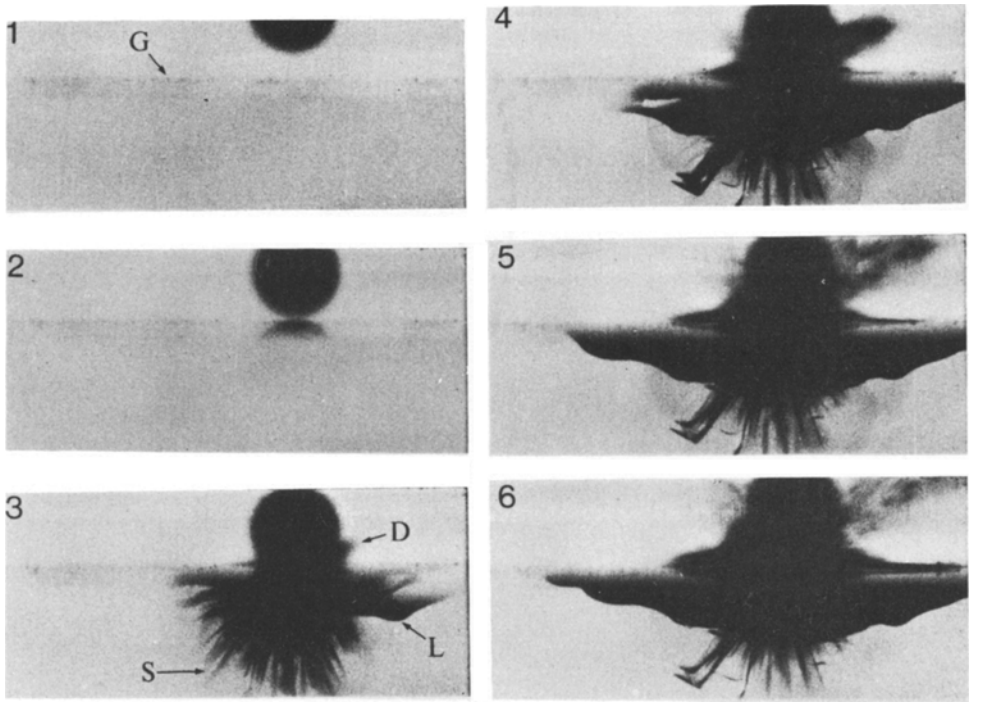

Figure 6 Impact of 0.8 mm diameter steel ball on soda-lime glass, G. Impact velocity 200 m sec^{-1}; framing interval 1 μsec. S, splinter cracks; L, lateral cracks; and D, glass debris.

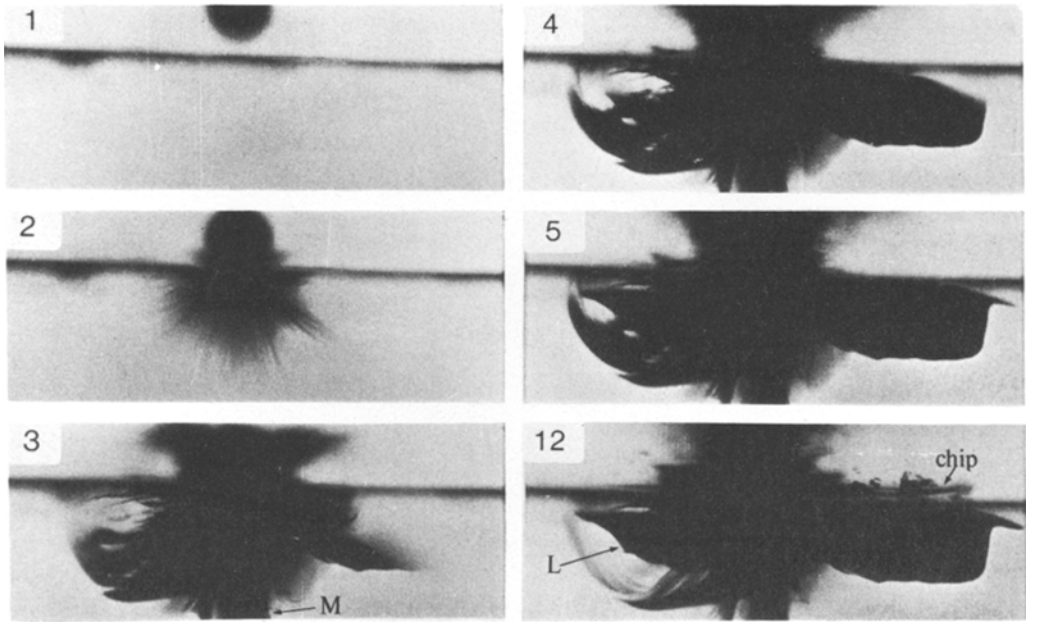

Figure 7 Impact of 0.8 mm diameter steel ball on soda-lime glass. Impact velocity 300 m sec^{-1}, framing interval 1 μsec. M, median crack; L, lateral crack.

beneath this compressive zone but without large flaws in this regions fracture is unlikely to initiate. However, as mentioned in Section 2, if plastic flow or crushing occurs there are strong tensional components at the plastic– or crushed–elastic interface beneath the impact site which could initiate these splinter cracks. The mean velocity of these splinter cracks is ~ 1500 m sec^{-1}, the terminal velocity of crack propagation in soda-lime glass. Some of these splinter cracks, particularly those adjacent to

the surface, tend to curve upwards and continue to propagate on unloading. These cracks behave in a similar manner to lateral cracks about pointed indenters on unloading. The deeper propagating splinter cracks radically change direction on unloading and continue to propagate for a short distance, for example frame 4 in Fig. 6. In Fig. 7 where the extent of crushing has been more significant than Fig. 6, even some of the deeper penetrating splinter cracks sweep back towards the surface on unloading. The velocity of these unloading cracks is only $\sim 300\,\mathrm{m\,sec^{-1}}$ which is much lower than initial loading cracks. Although the impact stress field is relaxing on unloading, the centrally crushed and deformed zone under the impact site does not recover elastically. This zone presumably provides the driving force for these laterally propagating cracks. Fracturing beneath the impact site is usually completed within 4 to 5 μsec, and the last frame in Fig. 7, 7 μsec after the previous frame, shows the detachment of a relatively large chip from the surface; the chip forming after the intersection of a lateral crack with the surface. Examination of the impact site microscopically after impact indicated no substantial differences from that observed during impact. In all cases debris, presumably pulverised glass, may be seen spraying from about the impact site at velocities of $\sim 600\,\mathrm{m\,sec^{-1}}$.

Other high speed photographic sequences confirmed the general features of the above observations, including the formation of well developed median cracks similar to the one in Fig. 7. On two occasions with slightly lower velocity impacts on fractured float glass surfaces no indentation fracture occurred, although a slight depression at the impact site was noted.

5.2. Variation of cone crack angle in pyrex with impact velocity

The variation of cone crack angle in pyrex with impact velocity for both 0.8 and 1.0 mm steel balls over the range 35 to 250 $\mathrm{m\,sec^{-1}}$ is shown in Fig. 8. Most of the results were obtained with the gas-gun and the angle of the cone crack was measured from transverse sections. Typical cross sections of cone cracks at high and low velocity are shown in Fig. 9. The data plotted in Fig. 8 is for both ball sizes, and within experimental scatter it appears to be independent of ball size. Also plotted in Fig. 8 is the cone crack angle for quasi-static indentations with a 1.0 mm ball.

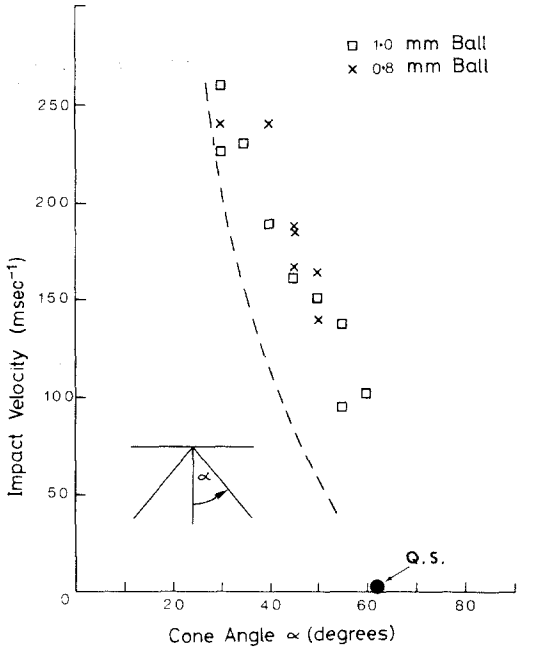

Figure 8 Variation of cone crack angle with impact velocity for 0.8 and 1.0 mm diameter steel balls on Pyrex glass. Broken line indicates predicted variation of cone crack angle with impact velocity, see text for details. Q.S. is the quasi-static cone crack angle.

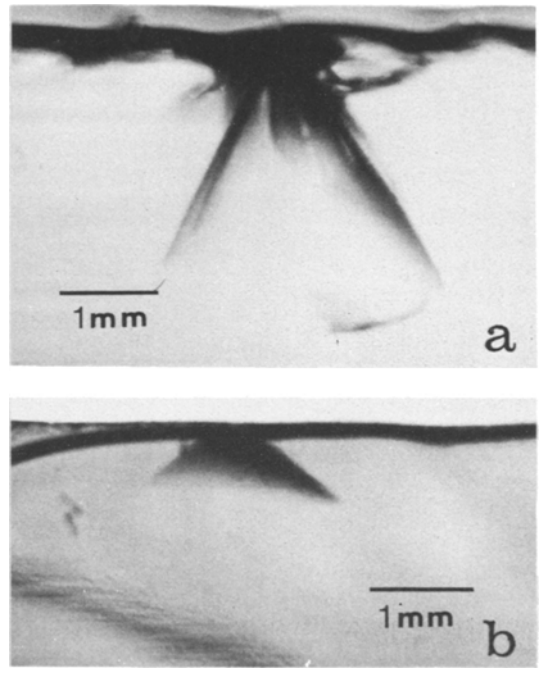

Figure 9 Cross sectional views of cone cracks in Pyrex glass at high (a) ($\sim 240\,\mathrm{m\,sec^{-1}}$) and low (b) ($\sim 95\,\mathrm{m\,sec^{-1}}$) velocity impact. The respective cone half angles are 35° and 55°. Note also that with the high velocity impact the cone crack has turned inwards on the right hand side.

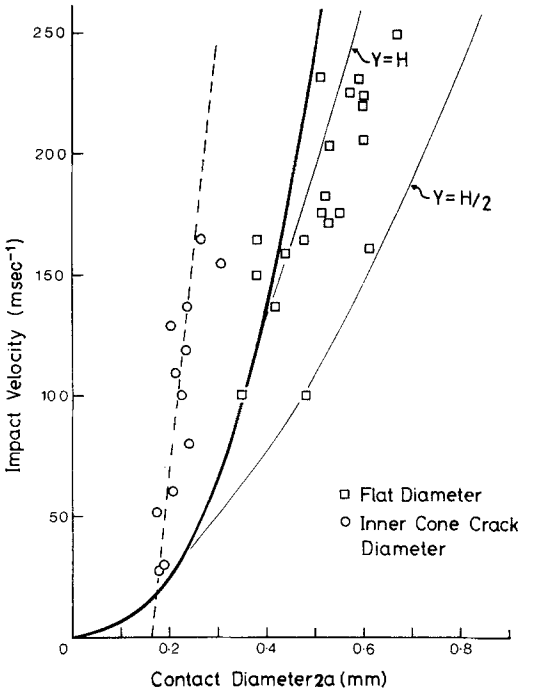

Figure 10 Variation with impact velocity of elastic diameter of contact, heavy line; inner cone crack diameter, broken line; observation of flat diameter on 1.0 mm steel spheres, □; and diameter of contact when plastic deformation of the sphere occurs when the yeild stress is H and $H/2$ respectively, faint lines.

The diameter of the surface trace of the cone cracks (generally there were at least two, depending upon the impact velocity, hereafter called inner and outer cone cracks) was also measured as a function of velocity, Fig. 10. At high velocities crushing occurred and the surface trace of the cone crack was obliterated. From Fig. 10 it appears that the inner cone crack varies only slightly with velocity until crushing occurs. This observation is in agreement with the limited observations by Adler [28] of glass spheres impacting glass and with the observations by Andrews [1] who found that the inner cone crack diameter was independent of the height from which the sphere was dropped. Also plotted in Fig. 10 is the elastic contact diameter as a function of velocity, Equations 1 and 4, and increase in diameter of contact when plastic deformation of the sphere occurs according to equation 9. The Vickers Hardness H_v of the sphere was 9.2 GPa, and the two plastic contact curves in Fig. 10, are for Y in Equation 9 equal to H_v and $H_v/2$. The diameter of the flat measured on the 1.0 mm ball as a function of velocity is plotted in Fig. 10, and although there is considerable scatter, the results do appear to fall between the curves for the two values of yield stress used. It is now possible, knowing the ratio of the inner cone crack diameter to maximum contact diameter, to predict the cone crack angle variation as a function of velocity from Fig. 1. The dashed line in Fig. 8 is the predicted cone crack angle variation with velocity and it agrees reasonably well with observation.

5.3. Time of contact and coefficient of restitution

Systematic variation of contact time with velocity could only be obtained with Pyrex glass, the soda-lime glass data showed considerable scatter. Fig. 11 shows that as the impact velocity increases the contact time decreases to a minimum approximately coincident with the onset of crushing and radial cracking, beyond which the time of contact increases. Also plotted in Fig. 11 is the theoretical variation of contact time with velocity according to Equation 8. The predicted time of contact appears to provide a lower bound for the present observations, although the increased time of contact at lower impact velocities is not understood. At higher impact velocities the longer contact times are expected because of plastic deformation of the sphere and crushing of the glass.

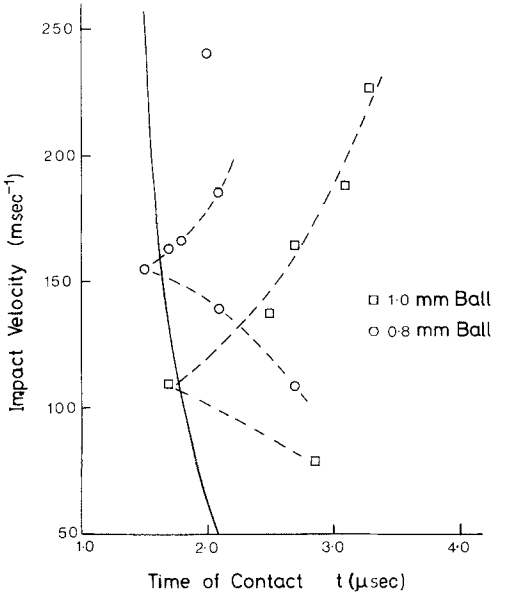

Figure 11 Variation of time of contact with impact velocity for 0.8 and 1.0 mm diameter steel spheres. The heavy line is the predicted theoretically variation according to Timoshenko and Goodier [21] for a 1 mm steel sphere.

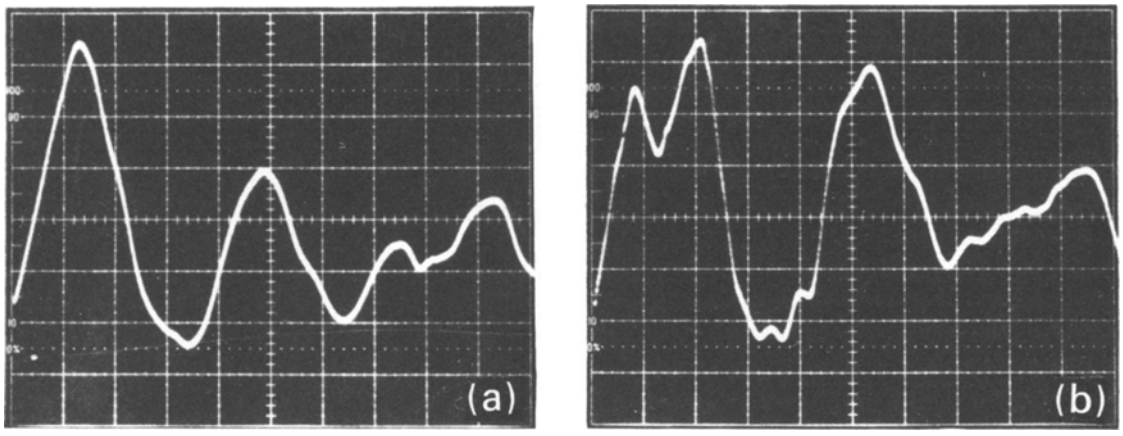

Figure 12 Typical oscilloscope traces of the transmitted compressional pulses resulting from impact on Pyrex glass with 1.0 mm diameter steel spheres. Trace (a) impact velocity ~ 80 m sec^{-1}; vertical scale 2V/div., horizontal scale 1 μsec/div. Trace (b) impact velocity ~ 165 m sec^{-1}; vertical scale 5V/div., horizontal scale 1 μsec/div. Note the sharp dip in trace (b) which was associated with a well developed cone crack.

Typical traces of the impact pulse recorded on the oscilloscope are shown in Fig. 12. Note the presence of a well-defined dip in the pulse in Fig. 12b (V ~ 165 m sec^{-1}) and the absence of the dip in Fig. 12a (V ~ 80 m sec^{-1}). This dip was associated with the formation of well-developed cone cracks and a slight amount of crushing and radial cracking. Tsai and Kolsky [6] reported a similar phenomenon but in their case they were monitoring surface Rayleigh waves whereas the pulses in Fig. 12 are the transmitted compressional waves.

From the rebound velocity determinations it was possible to determine the coefficient of restitution for both sizes of spheres on Pyrex glass, Fig. 13. There appears to be a distinct step discontinuity in the coefficient of restitution at the onset of crushing and radial cracking, it then drops very quickly as crushing becomes more severe. In one case where crushing was not observed the rebound velocity was substantially higher. These observations are confirmed by Tsai and Kolsky's [6] results which are also plotted in Fig. 13.

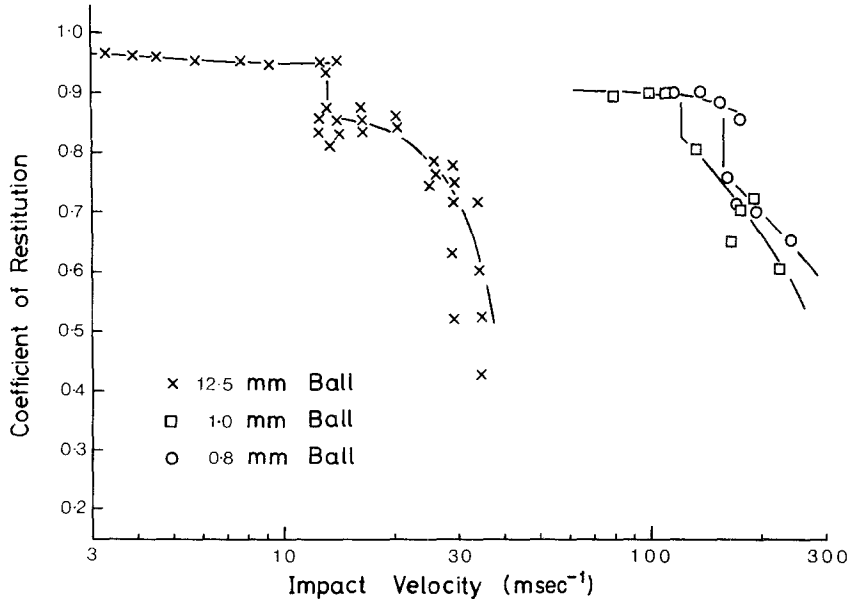

Figure 13 Variation of the coefficient of restitution with impact velocity for steel balls on glass. The 1.0 mm and 0.8 mm results are from the present study whereas the 12.5 mm results are replotted from Tsai and Kolsky's [6] paper.

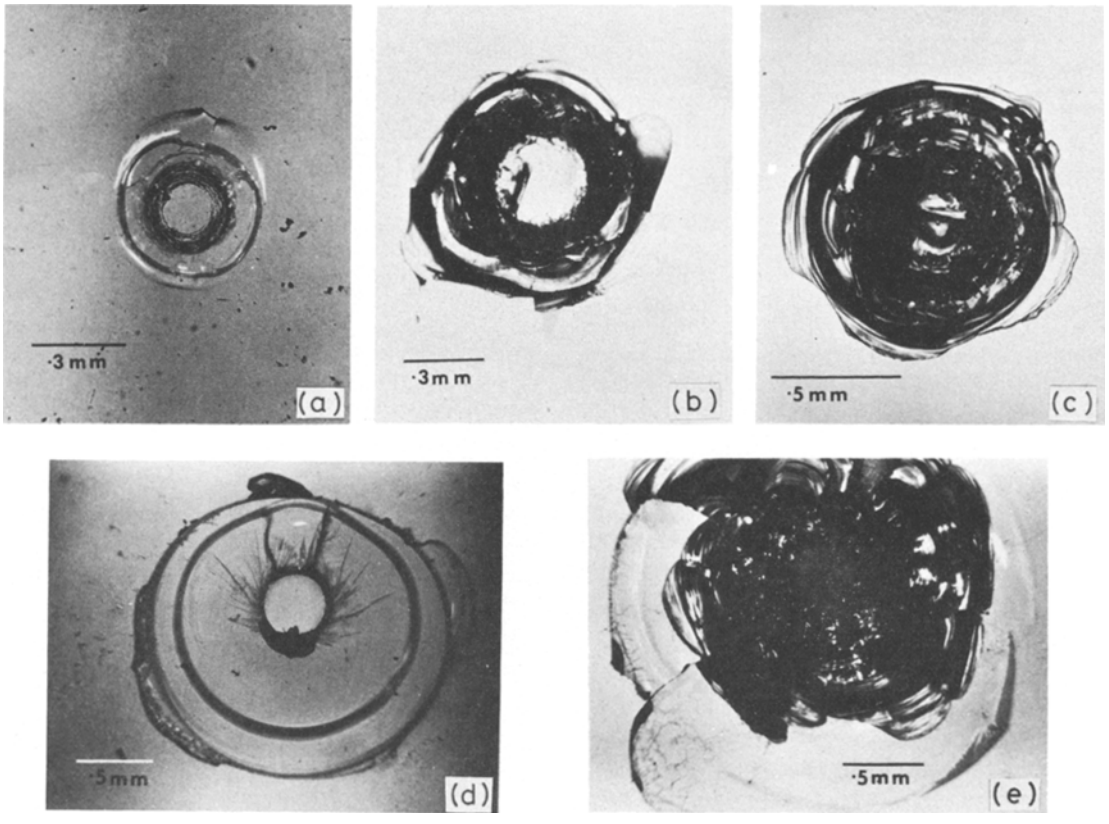

Figure 14 Observations of the surface cracking in Pyrex glass a, b, c, and soda lime glass d, e resulting from impact with 1.0 mm diameter steel balls at (a) 26 m sec^{-1}, (b) 105 m sec^{-1}, (c) 127 m sec^{-1}, (d) 165 m sec^{-1} and (e) 178 m sec^{-1}.

5.4. Surface features and depth of damage on impact

The surface features as might be expected vary with impact velocity and to some extent with the glass. For Pyrex below a critical velocity the only observation is the surface trace of the cone cracks, Fig. 14a. Above the threshold velocity a slight amount of crushing, radial and sometimes lateral cracking occurs at the edge of the contact area, Fig. 14b, and a higher velocities the complete contact zone is crushed and the cracking is more extensive, Fig. 14c. For soda-lime glass the transition from simple cone cracking to complete crushing and associated radial and lateral cracking appears to be more abrupt, Fig. 14d and e. For the 1 mm ball the transition from cone cracking to crushing occurs at ~ 160 to 170 m sec^{-1}. It might be expected that this transition velocity would be influenced by surface preparation, as it is for quasi-static cone crack formation.

Finally, the vertical extent of subsurface cracking beneath the impact site (usually cone crack depth) as a function of velocity is plotted in Fig. 15 for Pyrex glass. Also plotted is the predicted depth of damage, c, as proposed by Lawn *et al.* [29] according to the Roesler [4] equation for quasi-static conditions:

$$c = \frac{R_c}{\tan \alpha} = \left[\frac{P_m^2 K(\nu, \alpha) \sin \alpha}{2\Gamma E}\right]^{1/3} \Big/ \tan(\alpha) \tag{12}$$

where R_c is the radius of the base of the cone crack, P_m is the equivalent load from Equation 5, Γ the fracture surface energy $\simeq 4$ J m^{-2} for Pyrex and α is the angle of the cone crack, typically $\alpha = 63°$ for quasi-static indentations, and $K(\nu, \alpha) \sin \alpha$ is a constant approximately 1.4×10^{-3} for glasses. Equation 12 greatly underestimates the extent of damage because as shown in Section 5.2 the cone crack angle varies with velocity. However if one includes the variation of α with velocity then the modified form of Equation 12 is

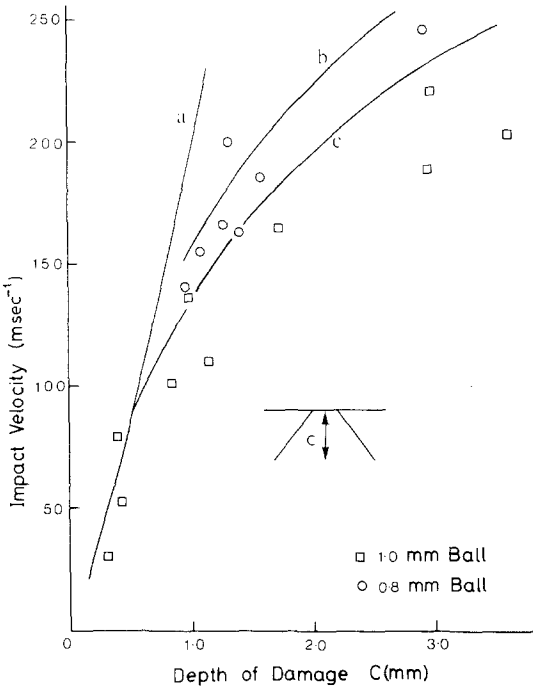

Figure 15 Variation of the depth of cracking in Pyrex glass as a function of impact velocity for 1.0 mm and 0.8 mm diameter steel balls. Also plotted is the predicted variation of cone crack depth according to Equation 12 for 1.0 mm diameter steel balls (a), and according to Equation 12a for 0.8 mm (b), and 1.0 mm (c) diameter steel balls.

$$c = \frac{R_c}{\tan \alpha(V)} = \left[\frac{P_m^2 K(\nu, \alpha) \sin \alpha(V)}{2\Gamma E}\right]^{1/3} \Big/ \tan \alpha(V). \quad (12a)$$

Unfortunately $K(\nu, \alpha)$ must be determined by finite element methods, Finnie and Vaidyanathan [30], but here it has been assumed constant $\simeq 10^{-3}$. Equation 12a fits the observations in Fig. 15 much better than Equation 12 although it still underestimates the data owing possibly to the assumption that $K(\nu, \alpha)$ is a constant, or crack growth continues on unloading.

This last observation is quite significant because it indicates that quasi-static analysis of impact damage greatly underestimates the depth of damage and consequently the residual strengths of brittle materials. A recent fracture mechanics analysis by Evans [31] of impact damage of silicon nitride underestimated the residual strength following cone crack initiation most probably because of the variation of cone crack angle with velocity.

6. Conclusion

The high speed photographic sequences of this study have shown that the impact damage is a two stage process. On the loading cycle the crack growth follows tensile stress trajectories, as predicted by the elastic loading stresses. Whereas crack propagaton on unloading is at present difficult to predict because of our limited knowledge of the residual stress. However the sequences do show the significance of the unloading cycle to the formation of chips and the removal of material. The high speed photographs have also shown the dramatic difference in behaviour of Pyrex and soda-lime glass to impact with small spheres and also suggest that interaction with the reflected stress pulse does not play a crucial role in the initiation of damage within the area of contact as proposed by Glenn [21]. For instance, crushing (splinter crack development) within the contact zone occurs within $\sim 1\,\mu$sec of contact, far less than the time for the reflected wave to return to the contact zone, $> 2\,\mu$sec. On the other hand the variation of cone crack with velocity only partially agrees with quasi-static predictions suggesting that dynamic considerations may be important.

The variation of cone crack angle with impact velocity is of immense significance because of its implications to erosion and strength degradation of brittle solids. Adler [28] has shown that solid particle erosion in Pyrex glass occurs by the interaction of cone cracks. A complete analytical description of this phenomenon would need to encompass the variation of cone crack angle with impact velocity as well as the occurrence of crushing, lateral and radial cracking. Moreover, the mechanisms of failure beneath the impacting sphere depends upon the intrinsic mechanical properties of the materials, as shown by the marked difference in behaviour of Pyrex and soda-lime glass. Strength degradation resulting from impact of brittle solids by small particles is also an important problem, an accurate assessment of the depth of damage being essential for one to determine either the fracture strength or lifetime of the damaged component in service. The present observations indicate a substantial increase in the depth of damage (flaw size) when impacted over that expected from quasi-static predictions. These and

other aspects of this work are being further pursued.

Acknowledgements

The Ministry of Defence (Procurement Executive) is thanked for a grant to the laboratory and the S.R.C. for financial support to one of us (MVS). J. E. Field, B. R. Lawn, and J. T. Hagan are thanked for comments on the manuscript, and I. M. Hutchings for help with the use of his gas-gun facility.

References

1. J. P. ANDREWS, *Proc. Phys. Soc. Lond.* **43** (1931) 18.
2. L. LONGCHAMBON, *C.R. Acad. Sci. Paris* **199** (1934) 1381.
3. J. P. A. TILLET, *Proc. Phys. Soc.* **B69** (1956) 47.
4. F. C. ROESLER, *ibid* **B69** (1956) 981.
5. F. AUERBACH, *Ann. Phys. Chem.* **43** (1891) 61.
6. Y. M. TSAI and H. KOLSKY, *J. Mech. Phys. Solids* **15** (1967) 263.
7. G. P. CHEREPANOV and V. B. SOKOLINSKY, *Eng. Fract. Mech.* **4** (1972) 205.
8. B. R. LAWN and M. V. SWAIN, *J. Mater. Sci.* **10** (1975) 113.
9. M. V. SWAIN and J. T. HAGAN, *J. Phys. D. Appl. Phys.* **9** (1976) 2201.
10. F. P. BOWDEN and J. E. FIELD, *Proc. Roy. Soc. Lond.* **A282** (1964) 331.
11. J. E. FIELD, *Phil. Trans. Roy. Soc. Lond.* **A260** (1966) 86.
12. L. A. GLENN, *J. Mech. Phys. Solid* **24** (1976) 93.
13. H. HERTZ, Miscellaneous papers (MacMillan, London 1895) Ch. 5.
14. M. T. HUBER, *Ann. Physik* **14** (1904) 153.
15. K. L. JOHNSON, J. J. O'CONNOR and A. C. WOODWARD, *Proc. Roy. Soc. Lond.* **A334** (1973) 95.
16. B. R. LAWN and T. R. WILSHAW, *J. Mater. Sci.* **10** (1975) 1049.
17. D. M. MARSH, *Proc. Roy. Soc. Lond.* **A282** (1964) 33.
18. R. HILL "Plasticity" (Oxford University Press, Oxford, 1950) p. 97.
19. K. E. PUTTICK, L. S. A. SMITH, and L. E. MILLER, *J. Phys. D. Appl. Phys.* **10** (1977) 617.
20. J. C. JAEGER, "Elasticity, Fracture and Flow", 2nd Edition (Methuen, London, 1962) p. 186.
21. S. P. TIMOSHENKO and J. N. GOODIER, "Theory of Elasticity" (McGraw-Hill, New York, 1970) p. 420.
22. S. C. HUNTER, *J. Mech. Phys. Solids* **5** (1957) 162.
23. H. L. OH and I. FINNIE, *ibid* **15** (1967) 401.
24. F. C. FRANK and B. R. LAWN, *Proc. Roy. Soc. Lond.* **A299** (1967) 291.
25. B. R. LAWN, T. R. WILSHAW and N. E. W. HARTLEY, *Int. J. Fract.* **10** (1974) 1.
26. F. P. MALLINDER and B. A. PROCTOR, *Phys. and Chem. Glasses* **5** (1964) 91.
27. M. M. CHAUDHRI, C. G. KNIGHT and M. V. SWAIN, 12th International High-speed photography Conference, Toronto, August 1976.
28. W. F. ADLER, *J. Non-cryst. Solids* **19** (1975) 335.
29. B. R. LAWN, S. M. WIEDERHORN and H. H. JOHNSON, *J. Amer. Ceram. Soc.* **59** (1976) 428.
30. I. FINNIE and S. VAIDYANATHAN, Proceedings of the Conference on Fracture Mechanics of Ceramics, Edited by R. C. BRADT, D. P. H. HASSELMAN and F. F. LANGE, Vol. 1 (Plenum Press, New York, 1974) p. 231.
31. A. G. EVANS, *J. Amer. Ceram. Soc.* **56** (1973) 405.
32. I. M. HUTCHINGS and R. E. WINTER, *J. Phys. E.* **8** (1975) 84.
33. C. J. STUDMAN and J. E. FIELD, *J. Phys. D. Applied Phys.* **9** (1976) 857.

Received 25 November 1976 and accepted 27 January 1977.